Characterization of a Photonics E-Field Sensor as a Near-Field Probe

Brett T. Walkenhorst[1], Vince Rodriguez[1], and James Toney[2]
[1] NSI-MI Technologies
Suwanee, GA 30024
[2] SRICO
Columbus, OH 43235
bwalkenhorst@nsi-mi.com

Abstract - In this paper, we explore the possibility of using a photonics-based E-field sensor as a near-field probe. Relative to open-ended waveguide (OEWG) probes, a photonics probe could offer substantially larger bandwidths. In addition, since it outputs an optical signal, a photonics probe can offer signal transport through optical fiber with much lower loss than what can be achieved using RF cables.

We begin with a discussion of the theory of the device followed by a summary of results of a photonics sensor that was tested in a spherical near-field (SNF) range. In these tests, data were collected with the photonics probe in the test antenna position to characterize various probe parameters including polarization discrimination, probe gain, effective dynamic range, and probe patterns. Results are presented along with discussions of some of the advantages and disadvantages of using a photonics probe in a practical system based on the lessons learned in the SNF testing.

Keywords—Near-Field Measurements, Optical E-field Sensors

I. INTRODUCTION

The open-ended waveguide (OEWG) probe is one of the most commonly used probes in near-field measurement systems. Its radiation pattern can be reliably described by a closed form equation and it is small enough to measure the antenna under test with minimal effects on the measured field. The probes are, however, not ideal for all applications. At lower frequencies, they become physically large and heavy, with some of the probes operating down to 500 MHz being about 14.5kg (32lbs) and as long as 1m (39in). The extra weight calls for a bigger scanner support and higher power requirements for the motors on the scanner. At high frequencies, the probes can be fragile and require mixers, multipliers, couplers, isolators and low-noise amplifiers (LNAs) to be mounted on the probe carrier to reduce the high frequency losses.

In recent years, photonic electric sensor systems have become available. These systems use a lithium niobate Mach-Zehnder interferometer (MZI) to sense the electric field. A laser that propagates via fiber-optic cable is modulated by the electric field incident on the crystal. An optical receiver is then used to extract the amplitude and phase of the electric field incident on the crystal. Figure 1 shows an example of such a sensor.

Figure 1. A Lithium Niobate MZI inside its package compared to a 25-cent US coin.

These sensors have extremely wide frequency bands, being able to sense fields as low as 1 Hz to as high as 20 GHz; though for a given sensor, the usable bandwidth may be somewhat smaller than that. For example, the probe testing reported in this paper indicates good response as low as 100 MHz and as high as 15 GHz, though the probe's response may be wider than that. The overall system bandwidth is typically limited by the optical detector. The sensors are very small (see Figure 1) and lightweight. Their construction is mainly dielectric, with the exception of some optional metallization to help improve the sensitivity.

In this paper, we describe the characteristics of these probes and discuss their applicability to near-field antenna measurement systems. We begin with a description of the photonics probe in Section II including the theory of its operation. In Section III, we describe the testing we performed and our characterization of the probe with reference to its applicability as a near-field measurement probe. Metrics we consider include sensitivity, cross-polarization discrimination, gain, and dynamic range. Conclusions are discussed in Section IV.

II. PHOTONICS ELECTRIC FIELD SENSOR

A. Background Theory and Operation

The basis of operation of a photonic electric field sensor is the linear electro-optic effect (the electric field-induced change

in refractive index in certain classes of dielectric materials). Lithium niobate ($LiNbO_3$) is the most widely used electro-optic material for this application due to its strong electro-optic effect, well developed fabrication technology, and commercial availability in large, high-quality wafers.

$LiNbO_3$ devices are typically designed such that both the optical wave and the modulating electric field are polarized along the crystal's z-axis to take advantage of the largest element of the electro-optic tensor, r_{33}. In this case, the relationship between the refractive index change, Δn_e, and the internal electric field, E_i, is [1]

$$\Delta n_e = -\frac{1}{2} n_e^3 r_{33} E_i \tag{1}$$

In an optical waveguide, the refractive index change of (1) translates to a phase difference in the optical wave. The phase difference is converted into a change in amplitude by the MZI. When used with a square-law photodetector (direct detection), the signal current is proportional to the transmitted optical power. The ideal (lossless) MZI transfer function (ratio of optical output to input power as a function of applied electric field) is

$$\frac{P_o}{P_i} = \frac{1}{2}\left(1 + \cos\left(\frac{\pi E_i}{E_\pi} + \Phi_0\right)\right) = \cos^2\left[\frac{1}{2}\left(\frac{\pi E_i}{E_\pi} + \Phi_0\right)\right] \tag{2}$$

where E_i is the internal field applied to the probe and E_π is the internal field required to produce a phase difference between the two arms of the interferometer of π radians. The value of E_π depends on the specifics of the sensor design. The operating point, Φ_0, is a function of the MZI geometry and dictates the small-signal response of the probe. It can be controlled actively by application of a DC bias, although this is typically not done in electric field sensing applications.

The standard expression for the gain of an analog fiber optic link can be applied to an electric field sensor system by substituting E_π in place of V_π (half-wave voltage) and adding a factor to account for the transformation from voltage applied to the source antenna to electric field within the crystal. The small-signal RF gain of the system in dB from the source antenna to the output of the photoreceiver, calculated as A in (3), depends on E_π, Φ_0, and the responsivity of the photoreceiver, $\mathcal{R}$, as [3]

$$A = 20\log\left[\frac{\gamma \sin\Phi_0 \mathcal{R} Z_{RF}}{E_\pi}\right] + 2(P_i - L) - 56\ \text{dB} \tag{3}$$

where γ is the ratio of the internal electric field to the voltage applied at the antenna input. This factor accounts for the antenna gain, distance from the antenna to the sensor, impedance of free space, and ratio of external to internal electric field. The last depends on the crystal shape and orientation, as well as the specifics of the electrode design, if any. P_i is the power of the laser in dBm and L is the optical insertion loss of the sensor, i.e. $P_i - L$ is the received optical power. The input impedance of the RF system following the photoreceiver is given by Z_{RF}, typically assumed to be 50 Ω.

Equation (3) shows that the response of the sensor itself is characterized by a figure of merit,

$$M = \frac{\gamma \sin\Phi_0}{E_\pi} \tag{4}$$

While γ and E_π can, in principle, be determined by modeling, Φ_0 can only be determined experimentally, since it arises from uncontrollable variations in material properties and device geometry and is temperature-dependent.

B. Dynamic Range

The dynamic range of the electric field sensor is limited at the low end by noise and at the high end by the nonlinearity of the MZI transfer characteristic. Gain compression is typically observed only at electric field amplitudes greater than 10 kV/m, a level not ordinarily reached in antenna measurements. Consequently, analysis of sensor dynamic range focuses on the minimum detectable field, defined as the field amplitude at which the signal to noise ratio is equal to 1.

The major contributors to noise in a photonic system are shot noise in the photoreceiver, relative intensity noise (RIN) in the laser, and Johnson (kT) noise in the receiver, amplifier, and measurement system [2]. Depending on the operating conditions and characteristics of the instrumentation, any one of these sources may be dominant. Shot noise-limited operation provides optimal performance, but this requires a sufficiently low-noise transimpedance amplifier, which presents a challenge at microwave frequencies.

In the shot noise-limited regime, the gain increases by 2 dB for each 1 dB increase in received optical power, while the noise power spectral density increases by 1 dB. The signal-to-noise ratio (and therefore the low end of the dynamic range) can be improved by increasing the laser power, provided that a photodetector is available that can receive the higher power level.

The minimum detectable field of a photonic sensor system is determined by immersing the probe in a known electric field and measuring the signal-to-noise ratio. One convenient setup for this type of measurement is a transverse electromagnetic mode (TEM) cell, or Crawford cell. A TEM cell is a parallel plate arrangement that provides a uniform electric field equal to the applied voltage divided by the plate separation, d. In terms of the RF power, assuming a 50 Ω termination,

$$E_{TEM} = \frac{\sqrt{(100\ \Omega) P_{RF}}}{d} \tag{5}$$

where P_{RF} is the power in watts. The assumption of a uniform field holds below the first resonant frequency of the TEM cell, typically around 1 GHz.

To characterize the probe, the signal power at a known input power and the noise power spectral density are measured with a spectrum analyzer. The minimum detectable field is then calculated as

$$E_{min} = E_{TEM} 10^{-SNR/20} \tag{6}$$

where SNR is the signal-to-noise ratio in a 1 Hz bandwidth. Since the noise power increases linearly with the measurement bandwidth, the minimum detectable field increases as the square root of the bandwidth. It is therefore expressed in units of V/m/√Hz

III. Characterization of the Probe

A. Characterization in a Test Cell

Prior to performing range measurements, the probe was characterized by measuring its response to a known field amplitude. The probe was placed in a 1 GHz TEM cell with a plate separation of $d = 6$ cm. Due to geometric constraints, the probe was oriented with its sensitive axis at 60° from the vertical. A -1.9 dBm, 300 MHz RF input signal was applied to the TEM cell, and the output signal from the sensor system was displayed on an RF spectrum analyzer. The signal power and the noise power in a 1 Hz bandwidth were measured as -45.1 dBm and -108.0 dBm, respectively, for an SNR of 62.9 dB. The minimum detectable field was calculated as

$$E_{min} = \frac{4.2\ \text{V/m}}{\cos 60^o} 10^{-62.9/20} = 1.5\ \frac{\text{mV}}{\text{m}\sqrt{\text{Hz}}} \qquad (7)$$

The response and noise level from 100 to 1000 MHz were measured using the spectrum analyzer's built-in tracking generator. Figure 2 shows the measured signal (blue), noise with RF source turned off (magenta), noise with the laser turned off (green) and noise with the low-noise amplifier turned off (red). The reduction in noise level when the laser is turned off indicates that the system is shot noise-limited.

B. Characterization of the Probe in an Anechoic Chamber

To characterize the probe, the spherical near-field range (SNF) at the NSI-MI Technologies facilities in Suwanee, GA was used. The range is approximately 20 ft (6.09 m) long by 15 ft (5.57 m) wide by 15 ft (5.57 m) tall. The side walls, ceiling, and the end-wall by the AUT positioner are lined with 8-inch absorber. The opposite end-wall has 24-inch absorber treatment. The floor is treated with a combination of 24-inch pyramidal absorber pieces and 18-inch walkway absorber. A photograph of the range is shown in Figure 3.

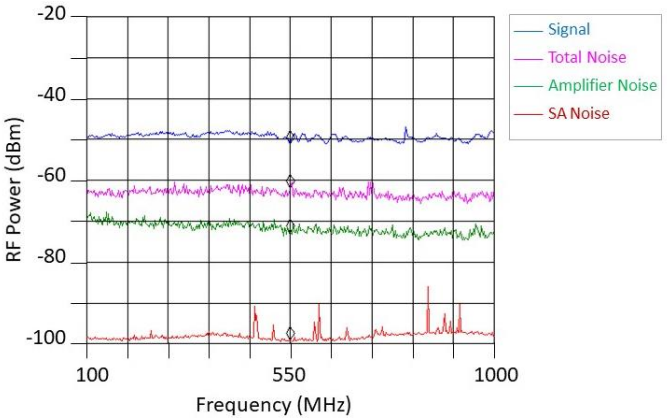

Figure 2. Spectrum analyzer measurement from 100 MHz to 1 GHz. Resolution bandwidth = 10 kHz.

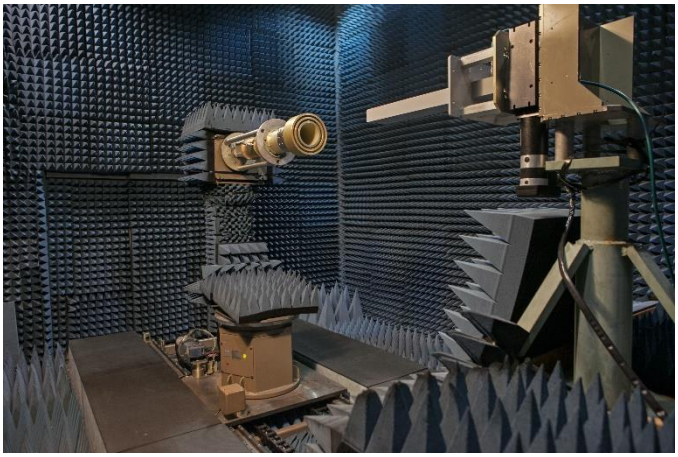
Figure 3. Anechoic SNF chamber looking towards the AUT end wall.

The photonics probe was mounted on the AUT positioner separated from the positioner structure by some absorber and a piece of rigid foam. A photograph of the mounting configuration is shown in Figure 4.

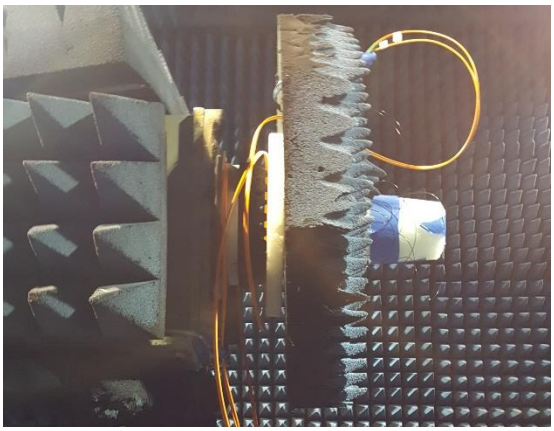
Figure 4. Mounting of the probe to the AUT positioner.

A Standard Gain Horn (SGH) was mounted as the range antenna. The measurement system, including equipment stack-up, is shown in Figure 5.

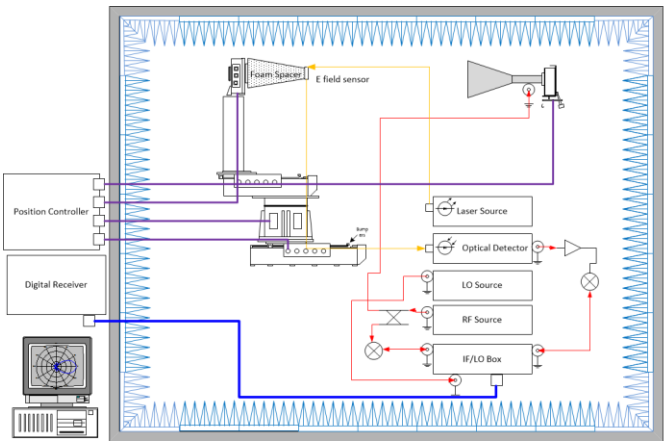

Figure 5. Test System.

A signal generator was used as the RF source. The output was routed via a directional coupler to the standard gain horn that illuminates the probe. The secondary signal from the directional coupler was input to a reference mixer. An additional signal source provided the local oscillator (LO) signal that was fed through an IF/LO distribution unit to the reference mixer. This part of the system provided a reference for the phase measurement. A laser source provided the optical signal to a fiber optic cable connected to the E-field (photonics) probe. At the E-field probe, the laser was modulated by the incident field and sent to an optical detector. The RF output of that detector was amplified by an LNA and then sent to a signal mixer where the LO signal from the IF/LO box mixed the received signal to IF. The IF signals were then routed to the digital receiver for further processing.

The AUT positioner configuration was a roll over mast over fixed offset over azimuth over floor slide. The range antenna was mounted on a fixed mast with a roll stage for polarization. All these axes were controlled by a position controller located outside of the range.

The first parameter measured was the polarization of the probe at three different bands: L-band, X-band, and Ku-Band. Different SGHs were used as range antennas and kept fixed as the roll stage on the AUT rotated the probe 180°. Figure 6 shows the cross-polarization level of the probe as it rotates through its roll axis at the three different bands. Three frequencies (low, middle, and high) per band are plotted. The cross polarization measured ranges from -36 to -38 dB for L-band, and -34 dB to -41 dB for X-band. For Ku-band, -45 dB was measured at 12.4 GHz, but for the middle and upper frequencies of the band, levels of -30 dB and -27 dB were measured, respectively. The plots in Figure 6 also show that there is a slight frequency-dependent tilt on the polarization of the probe. The null shifts about 5° around the 90° mark at L-band. At X-band, the location of the null is consistent, but tilted. At Ku-band, the shift is more pronounced, shifting as much as 15° from the 90° mark. Because the shift is not consistent, it cannot be completely explained by errors in the alignment of the probe when attaching it to the foam spacer.

Typical cross polarization for OEWG probes is better than -40 dB. For most of the frequencies measured, the optical probe is very close to this level. Where it falls short, the impact of reduced cross-pol may be assessed following methodologies such as those found in [4].

The probe's gain at X-band was found by measuring the boresight response of the photonics probe and an OEWG probe. Synthesized gain values for the OEWG probe were then used to perform gain substitution. In Figure 7, the synthesized OEWG values are plotted in blue, the computed gain values of the photonics probe in red, and the difference between them in yellow. Note that the apparent gain of the photonics probe is about 30-40 dB lower than the OEWG probe.

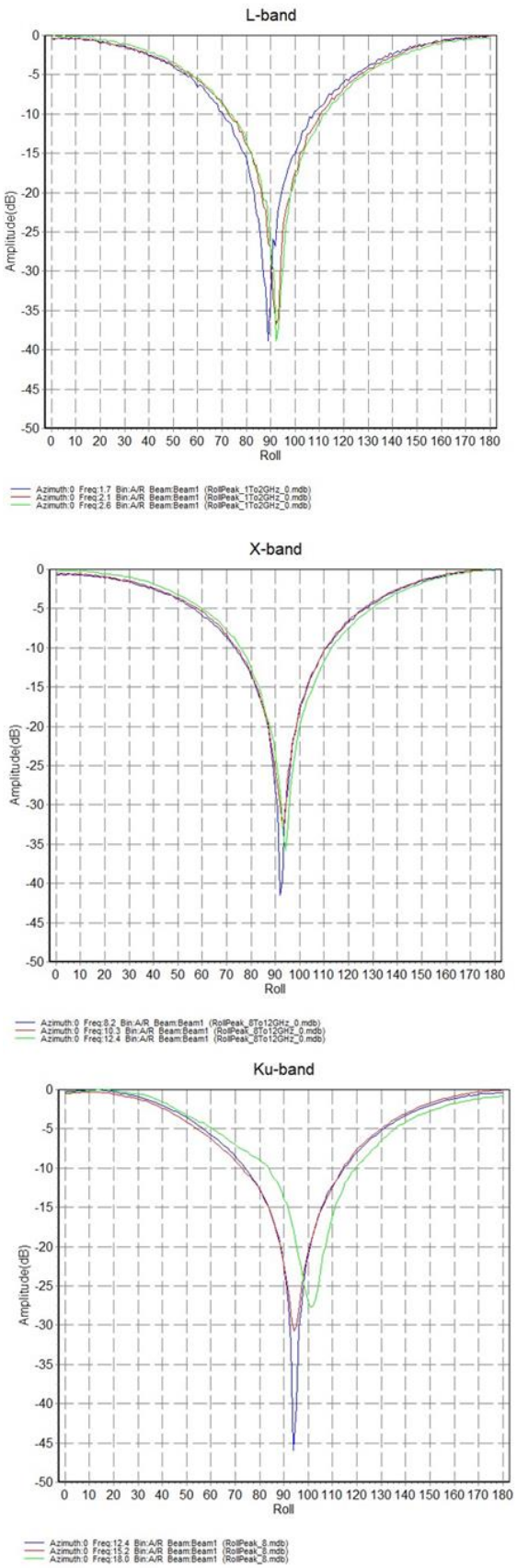

Figure 6. Cross polarization of the optical probe at three bands.

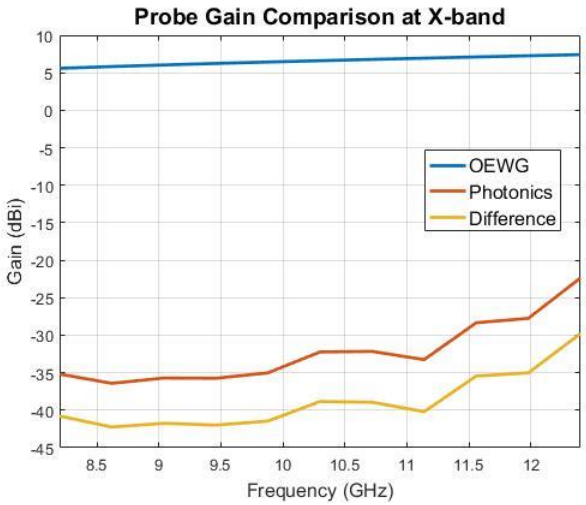

Figure 7. Measured gain of the photonics probe and OEWG probe.

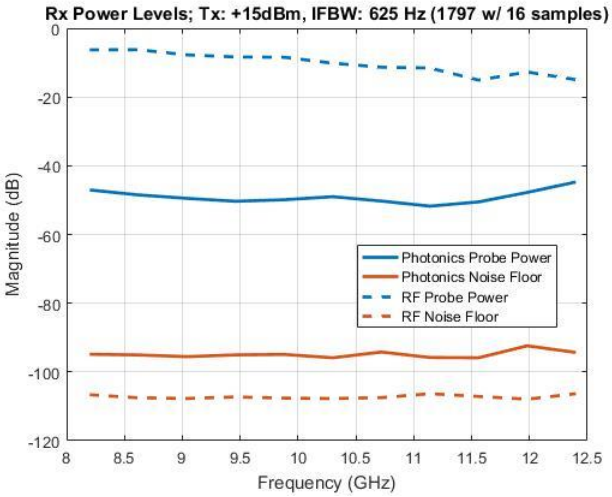

Figure 8. Received signal power and noise floor for photonics and OEWG probes.

The effective dynamic range for this specific test scenario was also found using the same boresight measurements used to find the gain. In Figure 8, the received power levels are plotted in blue and the measured noise floors are plotted in red. Figure 9 shows the difference between signal power and noise power for each of the probes. Note that the low gain of the photonics probe yields an effective dynamic range that is quite low. This can be improved by using a higher power laser, but this is practically limited to an improvement of about 10 dB, so the gain of this photonics probe will likely always be much less than that of the OEWG probe. Further improvements are achievable by optimizing the probe design for the field level and frequency range of interest.

Though the effective dynamic range of the photonics probe appears to be quite low, this is a result of the specific measurement scenario including range, test equipment, range probe, probe-to-probe distance, maximum transmit power, etc. However, the theory suggests that the actual dynamic range of the photonics probe is comparable to that of the OEWG probe and RF measurement system. This indicates that the photonics probe may work very well in high power measurement applications.

The probe pattern was also found by taking a complete spherical near-field raster and transforming to the far-field. The co-pol and cross-pol patterns are shown in Figure 10 and Figure 11, respectively.

Note the broad response of the co-pol pattern as a function of angle. While these patterns are preliminary, they indicate the possibility of simplifying transformations by minimizing the need for probe correction for all three canonical geometries.

Unfortunately, the broad pattern will also tend to over-illuminate undesirable portions of a chamber leading to a potential increase in observed stray signal levels. Although the details are not reported here, preliminary stray signal analysis of some of the collected data seems to support this supposition.

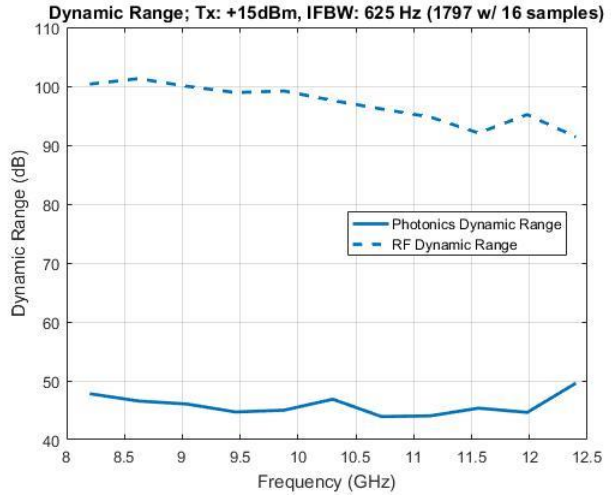

Figure 9. Effective dynamic range of photonics and OEWG probes for a specific test scenario.

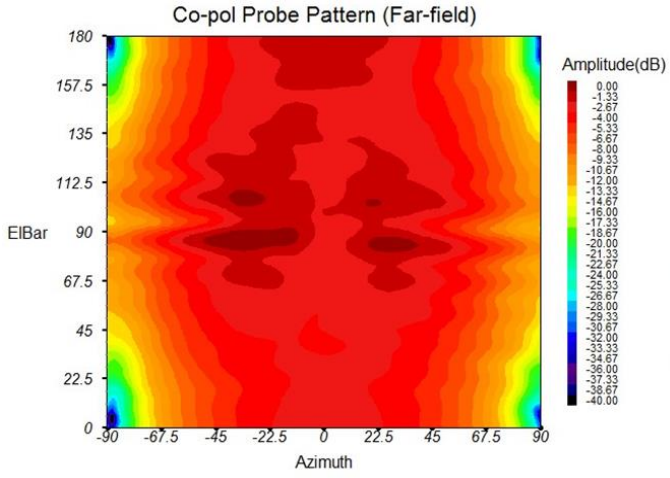

Figure 10. Co-pol pattern of photonics probe.

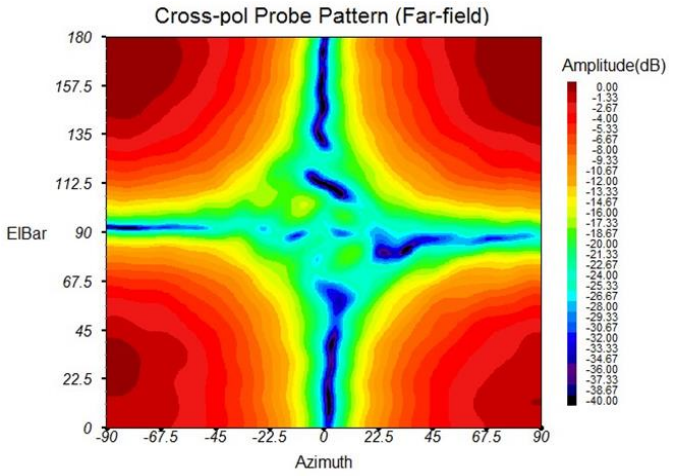

Figure 11. Cross-pol pattern of photonics probe.

IV. Conclusions

The results presented in this paper have shown that lithium niobate photonics sensors have the potential to be used as probes for near-field measurements. They exhibit adequate cross-polarization characteristics and broadband performance. Their primary advantages are extreme broadband response and low-loss signal transport via fiber optic cable.

The relative disadvantages of the photonics probe are very low gain and fairly broad beam patterns, which lead to poor power coupling and greater susceptibility to chamber-based stray signals. They are also receive-only probes, which can be a limitation for some measurement scenarios.

Overall, however, they offer a potential alternative to standard RF probes that may be useful for some applications. High power measurement applications, in particular, could significantly benefit from the probe's high-field capability.

The bulk of this paper has been an analysis of results collected with the photonics probe in the AUT position. Future work will include analysis and comparison of near-field and transformed AUT patterns using both an OEWG and the photonics probe in the probe position. Additional analysis on chamber effects related to the photonics probe's beam pattern will also be explored.

References

[1] H.C. Lefevre, The Fiber Optic Gyroscope, 2nd ed. (Boston: Artech House, 2014), p. 340.

[2] C.H. Cox, Analog Optical Links, Theory and Practice (Cambridge, U.K.: Cambridge University Press, 2004), pp. 159-173.

[3] J.E. Toney, Lithium Niobate Photonics (Boston: Artech House, 2015), p. 165.

[4] A. Newell, "Cross Polarization Uncertainty in Near-Field Probe Correction" *30th Annual Symposium of the Antenna Measurement Techniques Association (AMTA 2008)*, November 2008 Boston, MA.